3D Thermal Model of Laser Surface Glazing for H13 Tool Steel

I. R. Kabir[1,a)], D. Yin[2,b)], and S. Naher[1,c)]

[1]*Department of Mechanical Engineering and Aeronautics, City University of London, EC1V 0HB,UK*
[2]*Department of Material Processing Engineering, Henan University of Science and Technology, 263 Kaiyuan Avenue, Luoang, China*

Corresponding author: [a)]isratrumana@gmail.com
[b)]yindanqing@hotmail.com, [c)]drsumsun.naher@gmail.com

Abstract. In this work a three dimensional (3D) finite element model of laser surface glazing (LSG) process has been developed. The purpose of the 3D thermal model of LSG was to achieve maximum accuracy towards the predicted outcome for optimizing the process. A cylindrical geometry of 10mm diameter and 1mm length was used in ANSYS 15 software. Temperature distribution, depth of modified zone and cooling rates were analysed from the thermal model. Parametric study was carried out varying the laser power from 200W-300W with constant beam diameter and residence time which were 0.2mm and 0.15ms respectively. The maximum surface temperature 2554K was obtained for power 300W and minimum surface temperature 1668K for power 200W. Heating and cooling rates increased with increasing laser power. The depth of the laser modified zone attained for 300W power was 37.5μm and for 200W power was 30μm. No molten zone was observed at 200W power. Maximum surface temperatures obtained from 3D model increased 4% than 2D model presented in author's previous work. In order to verify simulation results an analytical solution of temperature distribution for laser surface modification was used. The surface temperature after heating was calculated for similar laser parameters which is 1689K. The difference in maximum surface temperature is around 20.7K between analytical and numerical analysis of LSG for power 200W.

1. INTRODUCTION

Laser surface glazing (LSG) is one of the surface treatment process to improve hardness, fatigue strength, wear resistance and corrosion resistance of engineering parts. After LSG treatment thin amorphous or semi crystalline layer forms over the surface with improved properties. No need of additional materials resulting into strong metallurgical bond thus makes this process beneficial from other treatments such as laser cladding, laser surface melting (LSM), laser transformation hardening, shock peening etc. However, higher heating and cooling rates involved in this process induce residual stress in the subsurface regions. This process is applicable in repairing and surface hardening of the parts in casting, automobiles and aeronautics industries [1-3]. To optimise the process parameters and improve the efficiency and reproducibility of LSG different theoretical models were developed. Previously, a thermal model of LSG for H13 tool steel using an analytical solution was developed. This model can predict relative temperature distribution and heating and cooling rates [4]. Some experimental works were done for LSG and laser surface melting (LSM) process on biomedical and automotive applications [5-6]. Analytical models for laser melting of ceramics tiles were developed to predict temperature distribution and depth of melt pool. Different methods such as Laplace transform, separation of variables and Green's function to solve partial differential governing equation of laser surface melting were used in different conditions. The analytical and numerical modellings support each other in verifying the results obtained from the simulation [7-12].

In this work, a 3D finite element (FE) model was developed extending from author's previous 2D modelling work of LSG for H13 tool steel [13]. Temperature distribution, depth of modified zone, heating and cooling rates were analysed from the 3D FE model. An analytical solution of this process using similar initial and boundary conditions

was utilized to predict temperature distribution from surface to subsurface region. The comparison of results from numerical models and analytical analysis was presented.

2. MODEL AND METHODOLOGY

Laser surface glazing represents as a transient heat conduction process. Therefore, the governing equation of this problem can be formulated from the 1st law of thermodynamics and Fourier's conduction principle. Equation (1) expressed the thermal phenomena underpinned in LSG process where k ($Wm^{-1}K^{-1}$) denoted thermal conductivity, C_p specific heat ($JKg^{-1}K^{-1}$) and ρ density (Kgm^{-3}) of the material. This equation described transient heat conduction in application of a constant heat flux rate on a particular location of surface.

$$\rho C_p \frac{\partial T}{\partial t} = k\left(\frac{\partial^2 T}{\partial x^2} + \frac{\partial^2 T}{\partial y^2} + \frac{\partial^2 T}{\partial z^2}\right) \tag{1}$$

The initial temperature was set up to 20°C as ambient temperature before starting the process, when time t=0. The boundary condition given in Eqs. (2), where Q_{laser} (W/m^2) was constant heat flux rate of laser beam. The heat loss due to convection and radiation was ignored.

$$-k\frac{\partial T}{\partial y} = Q_{laser} \tag{2}$$

Heat flux rate Q_{laser} was calculated from Eqs. (3) where P_{laser} (W) was power of laser beam, r_0 (m) was the laser beam radius. The total heat flux rate was multiplied with 0.3. This value represented the absorption coefficient of H13 tool steel for laser light [4, 12].

$$Q_{laser} = \frac{0.3P_{laser}}{\pi r_0^2} \tag{3}$$

Numerical Modelling

The 3D solid model of cylindrical specimen was created on mechanical APDL of ANSYS 15. The diameter of real cylindrical sample of H13 tool steel was 10mm and length was 100mm. To save meshing time half of the cylindrical specimen with 1mm length was utilized. As the irradiated laser beam was localised, therefore modelling with half-cylinder should not affect the output of the analysis. The laser beam of diameter 0.2mm interacted for 0.15ms over a particular area on the surface and created a circular molten puddle. An insight of the process was illustrated in Fig. 1a.

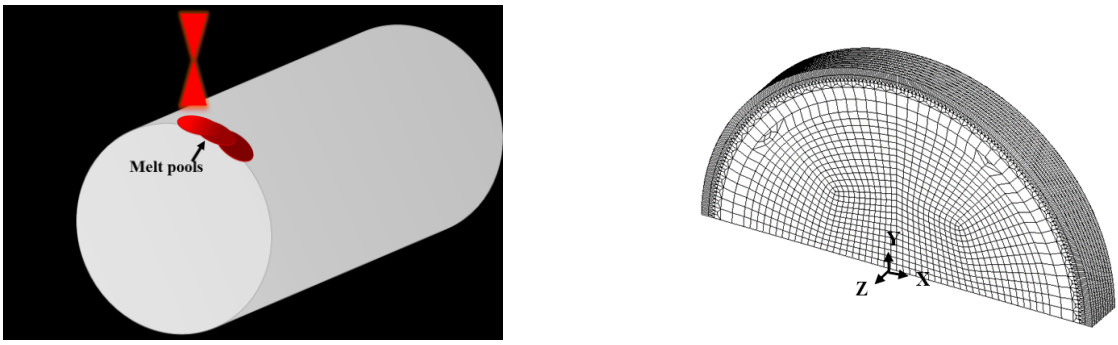

(a) (b)

FIGURE 1. (a) Schematic model of LSG of cylindrical specimen and (b) meshed model with the part of cylindrical sample

For finite element model Solid 70 element type was used which has 8 nodes and single degree of freedom as temperature. The surface and sub-surface regions were meshed finely whereas coarse meshes were kept in the core area (see Fig. 1b). Transitional meshing technique was used to reduce the number of elements resulting in increasing efficiency of the simulation process. The total number of elements for the half cylindrical model was 47060. The physical and thermal properties were input in the model which enlisted in table 1. Table 1 shows temperature dependent density, thermal conductivity, and specific heat. The properties above 2000°C were kept constant. From

table 1 it is obvious that the change in thermo-physical properties are very small after melting temperature (1454 °C). The data extrapolated from these values for each physical property did not have significant effect on surface temperature in this work. The time step size for this transient thermal process was taken 10^{-6} seconds. The governing equation and boundary condition were followed as Eqs. (1) and (2) for the solution.

TABLE 1. Thermo-physical properties of H13 tool steel as a function of temperature [14]

Temperature (°C)	Thermal conductivity (W m^{-1} K^{-1})	Specific Heat (J $kg^{-1}K^{-1}$)	Density (kg m^{-3})
25	28.6	447	7650
100	29.5	453	7650
500	35.39	519	7640
600	37.09	537	7550
1200	47.29	642	7100
1400	50.69	677	7000
1600	24.06	708	7000
2000	25	721	6900

Analytical Analysis

In the 2D analytical thermal analysis of LSG process the model was considered as semi-infinite model. Semi-infinite solid was idealized as a single identifiable surface which had two directions extended to the infinity. Any changes in this surface did not affect any other edges of the plane. A similar constant heat flux rate shown in Eqs. (3), was applied in one end of the surface caused 1D transient conduction along thickness. Thickness indicated the Y-direction downward from the surface of the cylinder (see Fig. 1b). Then the governing equation turned out to 1D transient heat conduction given in Eqs. (4)

$$\rho C_p \frac{\partial T}{\partial t} = k \frac{\partial^2 T}{\partial y^2} \tag{4}$$

The solution of the above differential equation was taken from Incropera [15]. Equation (5) presented the temperature distribution due to the irradiation of constant heat flux rate on the surface. Temperatures T(y,t) in this equation varied over thickness and time where T_i was the initial temperature of the material and erfc was the complementary error function. The temperature distribution for certain depth from the surface were plotted against distance in Y-direction and compared with the numerical results.

$$T(y,t) = T_i + \frac{2Q_{laser}(\alpha t/\pi)^{\frac{1}{2}}}{k} \exp\left(\frac{-y^2}{4\alpha t}\right) - \frac{Q_{laser} y}{k} \operatorname{erfc}\left(\frac{y}{2\sqrt{\alpha t}}\right) \tag{5}$$

Here, α (m^2/s) is the thermal diffusivity, is the ratio of thermal conductivity k and the product of density ρ and specific heat C_p.

3. RESULTS & DISCUSSION

Temperature distribution for different laser power from 3D numerical model were illustrated in Fig.2. The cross-section of temperature contour was shown in this pictures. The maximum surface temperature after heating for power 200W was 1668.67K and was 2554.54K for 300W. Comparing with 2D numerical case the maximum surface temperatures achieved from 3D case were 71K higher for 200W and 22K higher for 300W [13]. This was probably due to the increased surface heat flux in the 3D model. In 3D model heat flux from laser beam was applied over an area equal to beam's surface area rather than a line. This could accumulate more heat on the surface resulting higher surface temperature. On the other hand in 3D case the dimensional effect of conduction also accounted. Both effects balanced the surface temperatures resulting into higher values than the 2D model for both power levels.

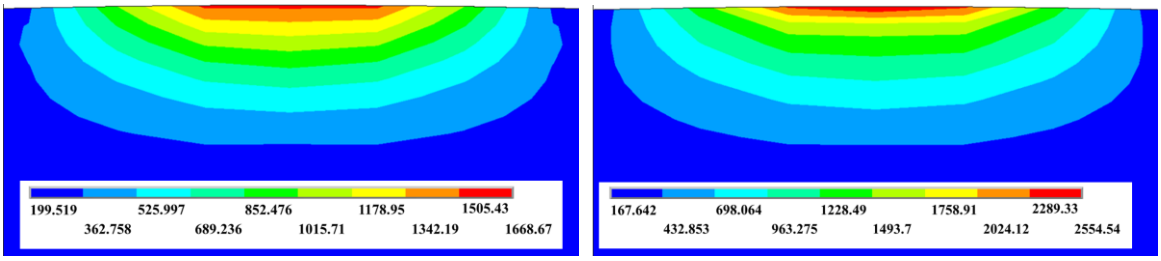

(a) (b)

FIGURE 2. Temperature distribution after heating for laser power (a) 200W and (b) 300W at constant beam width 0.2mm and interaction time 0.15ms

The depths of melt pool and heat affected zone (HAZ) were approximated from the temperature contours and demonstrated in Fig.3. Melting did not occur at 200W as the maximum temperature 1668K remained below the melting point (1727K). Therefore only HAZ was achieved of about 30µm depth. For power 300W melting happened and the depth of melt pool was 10µm. HAZ was calculated 27.5µm from the plot in Fig. 3b. Although total depth of HAZ were similar for both 2D [13] and 3D cases, the depth of melt pool was larger in 3D case. Around 2.5µm increment of the depth of melt pool for 300W was observed. This was also because of the greater accumulation of heat flux and higher maximum surface temperature arisen in 3D case.

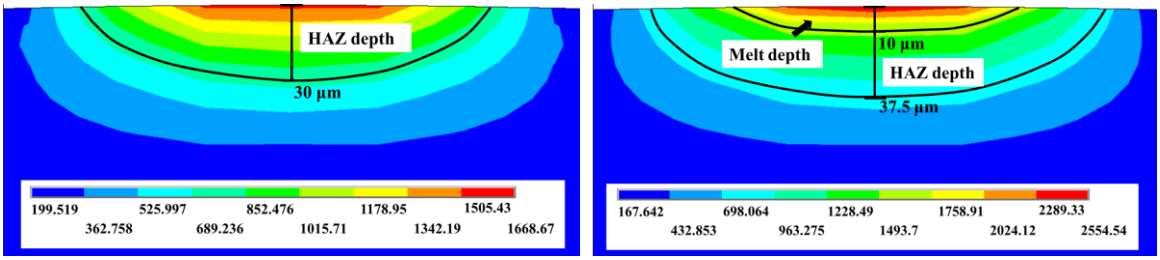

(a) (b)

FIGURE 3. Depth of melt pool and heat affected zone (HAZ) for (a) power 200W and (b) power 300W

The temperatures against time were plotted for both 200W and 300W in the Figs.4a and 4b. Thermal cycles at three different depths, A (on surface), B (7.5µm) and C (15µm) from the surface were plotted for both power levels. Then average heating and cooling rates were calculated from these figures.

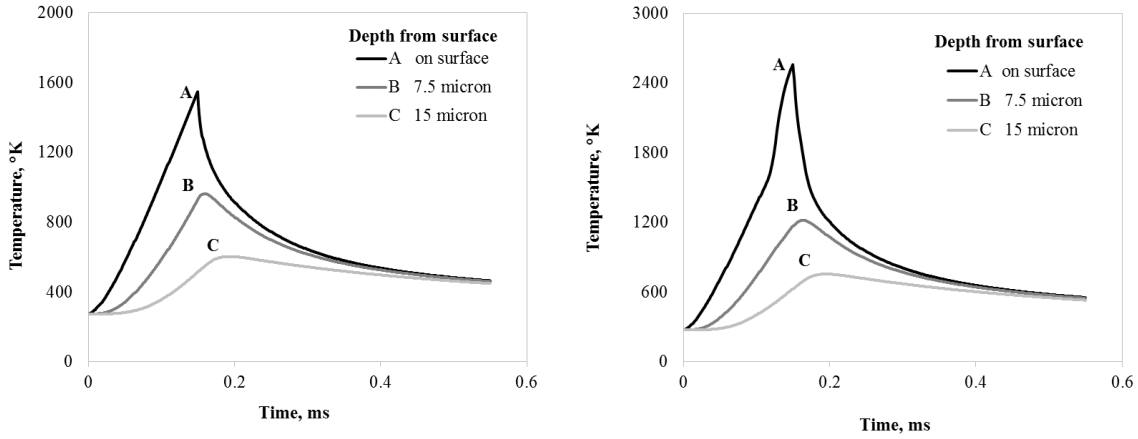

(a) (b)

FIGURE 4. Heating and cooling cycle at three different depths from surface for laser power (a) 200W and (b) 300W

This thermal cycles graphs can be further used to estimate possible phase fractions by superimposing critical isothermal temperature lines for phase transformation as done in [13, 14]. Table 2 showed heating and cooling rates of the surface (curve A) for different power levels. The corresponding heating rates for 200W and 300W laser power were 8.7×10^6K/sec 1.6×10^7K/sec. Cooling rates were achieved 3.4×10^6K/sec and 6.5×10^6K/sec for 200W and 300W respectively. Both rates increased with increasing power. Both heating and cooling rates were slightly higher than the 2D model because of higher maximum temperature obtained in 3D case [13].

TABLE 2. Heating and cooling rate on surface (A curves, Fig. 4a and 4b) for different power

Power	200W	300W
Rate of Heating, K/s	8.7×10^6	1.6×10^7
Maximum Rate of Cooling, K/s	3.4×10^6	6.5×10^6
	(Temp range, K: 1549-505)	(Temp range, K: 2554-612)

The temperature distribution calculated form analytical solution [see Eqs. (5)] and from both 2D and 3D numerical models were plotted in Fig.5 for power 200W. Temperatures against thickness (referred to downward y-direction) up to 60 micron were illustrated in this figure. The beam diameter and interaction time were kept constant at 0.2mm and 0.15ms respectively. Constant thermal properties with constant heat flux rate were used in analytical calculations. In case of numerical models temperature dependent thermal properties were used. For 2D numerical case line heat source and for 3D area heat source were applied. The maximum surface temperature after heating for 3D and 2D numerical models were 1668.7K and 1597.1K respectively. Surface temperature in 3D greater than 2D. This is because of the higher accumulation of heat in 3D. For analytical case, the maximum surface temperature was 1689.4K. Analytically obtained temperature was 20.7K higher than 3D and 92.3K higher than 2D numerical models. These increments in temperature might be because of the constant thermal properties used in analytical calculation. Author ensured the increment in temperature numerically for constant thermal properties. Because of the approximations in terms of heat distribution and semi-infinite solid model also could bring some discrepancies between analytical and numerical methods.

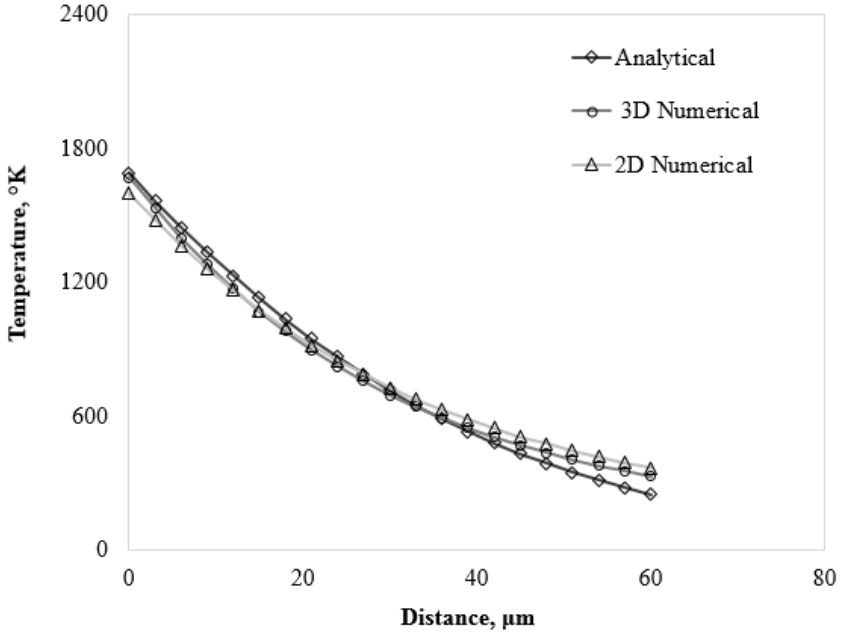

FIGURE 5. Temperature distribution from surface to the depth (downward Y-direction) for 200W laser power from analytical analysis and numerical models

4. CONCLUSIONS

A 3D finite element thermal model of laser surface glazing for cylindrical specimen was successfully extended and developed from 2D model. The maximum surface temperature, melt pool depth and heating and cooling rates were derived for 200W and 300W laser powers with 0.2mm beam width and 0.15ms interaction time. For 200W, maximum surface temperature (1668K) did not reach to melting point (1727K). The maximum surface temperature found (2554K) for 300W power was above melting point of H13 tool steel. The heating and cooling rates increased with increasing laser power. Author found small HAZ for 300W (27.5μm) than 200W (30μm). Molten layer of 10μm depth was found for 300W.The surface temperatures from 3D model than 2D model was observed maximum 4 percent. Therefore, dimensional effects can be ignored for the simulation of this process. However, for better accuracy author suggested the 3D modelling although it costs simulation time. An analytical solution of transient conduction process for semi-infinite solid was utilized to understand and compare the numerical simulation of LSG. The surface temperature obtained from analytical solution was 20.7K higher than the 3D numerical model. The difference in maximum surface temperature after heating could due to be the 1D approximation with constant thermal properties.

ACKNOWLEDGMENT

The work described in this paper has been supported by INTACT project of Erasmus-Mundus (Grant agreement reference: 2013-2829/001-001-EM Action2-Partnerships), and Department of Mechanical Engineering and Aeronautics of City University London. The author would be grateful enough to Dr. Ranjan Banerjee, Professor of Structural Dynamics in City University London, for his valuable guidance in developing the FEM thermal model.

REFERENCES

1. S. N. Aqida, S. Naher, and D. Brabazon, in *AIP Conference Proceedings*, **1353**, pp. 1081–1086 (2011).
2. E. Chikarakara, S. Naher, and D. Brabazon, *Appl. Phys. A Mater. Sci. Process.*, **101**, pp. 367–371 (2010).
3. J. Yang, S. Sun, M. Brandt, and W. Yan, *J. Mater. Process. Technol.*, **210**, pp. 2215–2222 (2010).
4. S. N. Aqida, S. Naher, and D. Brabazon, *Key Eng. Mater.*, **504–506**, pp. 351–356 (2012).
5. E. Chikarakara, S. Naher, and D. Brabazon, *Surf. Coatings Technol.*, **206**, pp. 3223–3229 (2012).
6. A. R. Zulhishamuddin, S. N. Aqida, and E. A. Rahim, *in AIP Conference Proceedings*, **1769**, pp 30004(1-6) (2016).
7. A. Peligrad, E. Zhou, D. and Morton, and L. Li, *Opt. Laser Technol.*, **33**, pp. 7–13, (2001).
8. B. S. Yilbas, *Int. Commun. Heat Mass Transf.*, **20**, pp. 545–555 (1993).
9. J. F. Li, L. Li, and F. H. Stott, *Int. J. Heat Mass Transf.*, **47**, pp. 1159–1174 (2004).
10. Q. Peng, *Appl. Math. Model.*, **40**, pp. 4129–4135 (2016).
11. H. G. Woo and H. S. Cho, in *Proceedings of the Institution of Mechanical Engineers, Part B: Journal of Engineering Manufacture*, **213**, pp. 695–712, (1999).
12. D. Sands, "Pulsed Laser Heating and Melting," in *Heat Transfer - Engineering Applications*, edited by Professor Vyacheslav Vikhrenkp (In Tech, 2011), pp. 47–52.
13. I. R. Kabir, D. Yin, and S. Naher, *in AIP Conference Proceedings*, **1769**, pp 110003(1-6) (2016).
14. P. Farahmand, P. Balu, F. Kong, and R. Kovacevic, in *ASME International Mechanical Engineering Congress and Exposition*, pp. 1–12 (2015).
15. F. P. Incropera and D. P. Dewitt, "Semi-Infinite Solid", in *Fundamentals of Heat and Mass Transfer*, 7th ed. (John Wiley and Sons, 2011), pp 310-313.